NURETH14-237

SIMULATING THE FLUID-STRUCTURE INTERACTION OF A FLEXIBLE TUBE IN AN ARRAY OF RIGID TUBES

D. Warnica¹, M. Maleki¹, A. Hariri¹, and H. Feldman²¹ Hatch Ltd., Mississauga, Ontario, Canada

² Electric Power Research Institute, Charlotte, North Carolina, USA

Abstract

Two important single-phase mechanisms for flow-induced vibration of heat-exchanger tube bundles were used to demonstrate the capabilities of commercial software to simulate unsteady fluid-structure interactions (FSI). Reasonable agreement was obtained between the FSI simulations and experimental data for the onset of fluidelastic instability. There was also reasonable agreement between the FSI simulations and empirical correlations for the dynamic tube response to random turbulence excitation. Additional benefits of performing FSI simulations were the ability to characterize important features of the unsteady flow fields and hydrodynamic parameters such as viscous damping coefficients, which would otherwise require elaborate experimental measurements.

1. Introduction

Recent advances in computational methods and computing hardware have made possible the simulation of detailed characteristics of fluid-structure interactions in heat-exchanger tube bundles.

Schroder and Gelbe (1999) [1] simulated the flow-induced vibration of a single flexible tube, a flexible tube row, and a flexible tube bundle using a STAR-CD flow solver coupled to a simple structural-dynamic program to simulate tube translations or coupled to a finite-element program to simulate tube deflections. A variety of unsteady RANS (k-ε) turbulence models were tested to select the most appropriate model to represent fluid-elastic interactions and critical velocities for the onset of instability. Reynolds (Re) numbers were as high as 140,000.

Kuehlert et al. (2006) [2] simulated flow-induced vibrations of single tubes and tube arrays in cross flow using a FLUENT flow solver coupled to an ABAQUS structural solver. Deflections of the tube arrays were considered using pinned-end constraints. Large Eddy Simulations (LES) were performed for tube bundles with Re equal to 100,000. Periodic boundary conditions were applied to a cell around a single tube to represent a tube array, so that the tube was assumed to vibrate in phase with an infinite array of other vibrating tubes. Forces at the tube centre were assumed to act over the entire tube length. These unrealistic assumptions were made to reduce computational effort, but may have limited accuracy of the results.

The objectives of the current work are to demonstrate the capabilities of commercial software to simulate two important mechanisms of flow-induced vibration (FIV) in heat-exchanger tube bundles, the onset of fluid-elastic instability and the tube response to random turbulence excitation. These results help validate FSI simulations for practical applications involving these FIV mechanisms.

2. Onset of fluid-elastic instability

2.1 Methodology

The onset of fluid-elastic instability of a flexible tube in a rigid array is demonstrated using the FSI capabilities of ANSYS software release 12.0, but other commercial software are also available for this type of application. A two-way, coupled FSI analysis is performed by solving the transient governing equations of fluid and structural dynamics. The governing equations are solved iteratively in a sequential segregated manner to obtain implicit transient solutions. A transient two-way FSI simulation therefore has three levels of iterations. The fluid and solid fields are solved at the inner field loop by CFD and FEA solvers. Loads and displacements are then updated at the FSI interface between the fluid and solid meshes until the individual field solutions and the interfacial loads and displacements converge at each time step. The time is then advanced to obtain the overall results of a transient FSI simulation.

2.1.1 Computational domain

The rotated triangular tube array (60°) shown in Figure 1 is selected for the geometry. To reduce simulation times, the computational domain is minimized as a single flexible tube in a rigid array of four tubes, which is subject to uniform crossflow (on average) over the entire tube length. Periodic boundary conditions account for the influence of neighbouring tubes that are not part of the computational domain. The flexible tube at the centre of the computational domain is therefore assumed to be vibrating in phase with an infinite column of other flexible tubes. The rigid tubes at the four corners of the computational domain are assumed to be in parallel columns of rigid tubes.

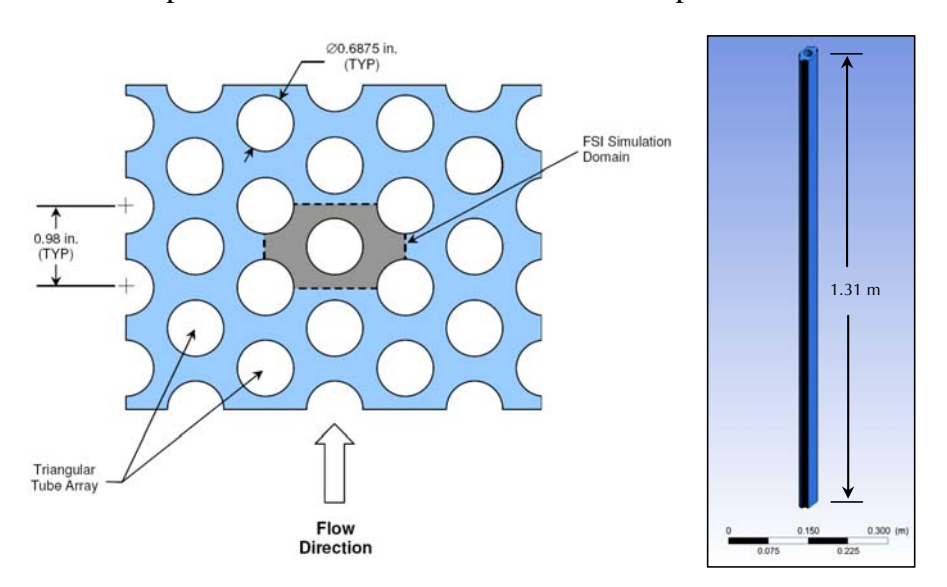


Figure 1 Computational domain.

The central tube is clamped at one end and pinned at the other end to represent constraints of the tube sheet and first tube-support plate, respectively. The four tubes at corners of the computational domain are entirely rigid and clamped at both ends. The tube pitch and outside diameter are 0.98 in (0.0249 m) and 0.6875 in (0.0175 m), respectively, for the triangular arrangement. Material properties are those of Alloy 600.

The 14th International Topical Meeting on Nuclear Reactor Thermalhydraulics, NURETH-14 Toronto, Ontario, Canada, September 25-30, 2011

The length of the computational domain corresponds to the tube length (L=1.31 m), which is selected (using Connors' equation [3]) for the onset of fluid-elastic instability to occur at a superficial crossflow velocity (V_s) of approximately 0.3 m/s. Connors' equation may be written as follows:

$$\frac{V_{P,C}}{fD_o} = C\delta_m^{\ a} \tag{1}$$

where f is the natural frequency of tube vibration, and δ_m is the mass-damping parameter:

$$\delta_m = \frac{2\pi\xi m_t}{\rho_0 D_o^2} \tag{2}$$

 D_o is the tube outside diameter, m_t is the mass per unit length, and ρ_0 is the fluid density. A suggested average constant coefficient (C=3.3 [3]) is used in the empirical correlation represented by Eq. (1), which is an industry accepted value that helps to define an approximate boundary condition for the crossflow velocity. The damping ratio ($\xi = 0.015$) for estimating the tube length is an assumed value of viscous damping in single-phase liquids, but this parameter is a function of the flow fields being simulated. The tube mass per unit length accounts for the mass of fluid inside the tube and the virtual mass of fluid vibrating outside the tube, in addition to the tube mass itself.

2.1.2 Mesh characteristics

The fluid and solid domains are independently meshed and modelled, as shown in Figure 2. The solid domain has a structured mesh with hexahedral elements through the material thickness (0.001 m) of the flexible tube and 41 elements around the circumference, so the aspect ratio in the 2-D cross section of the tube is approximately 1.3. Four hundred (400) elements are used along the tube length, so the aspect ratio in that direction is approximately 3.3. This mesh size is sufficient to characterize both the natural frequency and deformation of the flexible tube, which are relatively insensitive to further mesh refinement. The fluid domain has a multi-block structured mesh of hexahedral elements with an O-grid around the outside of each tube and H-grids in the interstitial spaces between tubes. The near-wall grid spacing of the O-grid is selected for a y+ (y-plus) $\cong 20$ at a velocity of 0.75 m/s, which is a non-dimensional distance from a wall [4]. The actual y+ values vary depending on local velocities around tubes. The grid expansion ratio of the O-grid is 1.2 in the radial direction so the aspect ratio of the near-wall grid spacing is approximately 45. There are 3,858 nodes in the 2-D cross section of the fluid domain and 1,547,058 nodes in the full model. This relatively coarse mesh with high aspect ratios is used to reduce computational effort and simulation times, but grid refinement may be required to obtain more accurate results.

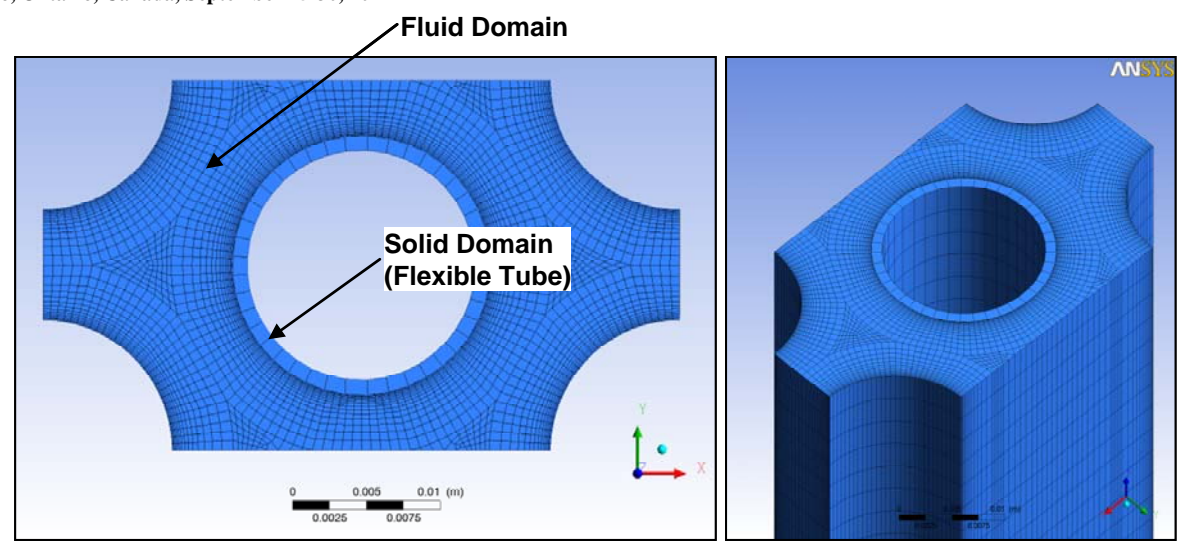


Figure 2 Computational mesh.

2.1.3 Fluid and tube properties

Fluid properties are based on those of saturated water at 284.9°C and 6.9 MPa. Mechanical properties of the tube are based on Alloy 600 at the fluid temperature.

A modal analysis using ANSYS Mechanical software was used initially to identify the predominant modes of tube vibration for the single-span, clamped-pinned constraints of the FSI simulations. The mass participation of the first (fundamental) mode was 74.0% at 29.6 Hz, which indicates that this mode of vibration should dominate the dynamic response of the tube. Figure 3 shows the mode shape of the first mode of vibration and its location of maximum tube deflection at an elevation of 0.75 m above the tubesheet. The relative influences of higher modes are also considered in the FSI simulations because a full solution is obtained for the system dynamics.

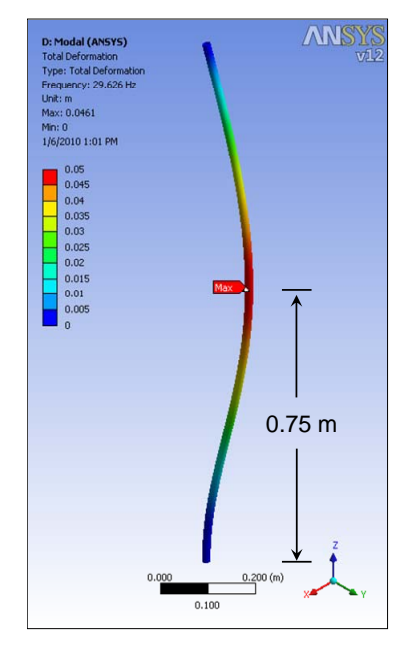


Figure 3 Tube deformation of first mode of vibration.

2.1.4 Boundary Conditions

The fluid and solid domains are shown in Figure 4 with some of the prevailing boundary conditions. Translational periodic boundaries are used on all sides to represent the flow field in a spatially periodic region around a single tube of a much larger tube bundle, which would exist in crossflow well away from the bundle inlet. The periodic boundary at the inlet is specified with a constant mass flow rate, corresponding to the product of the superficial velocity (0.75 to 1.5 m/s), fluid density, and total cross-sectional area of the computational domain. The outside surface of the central tube is the FSI interface for coupled loads and displacements between the fluid and solid elements.

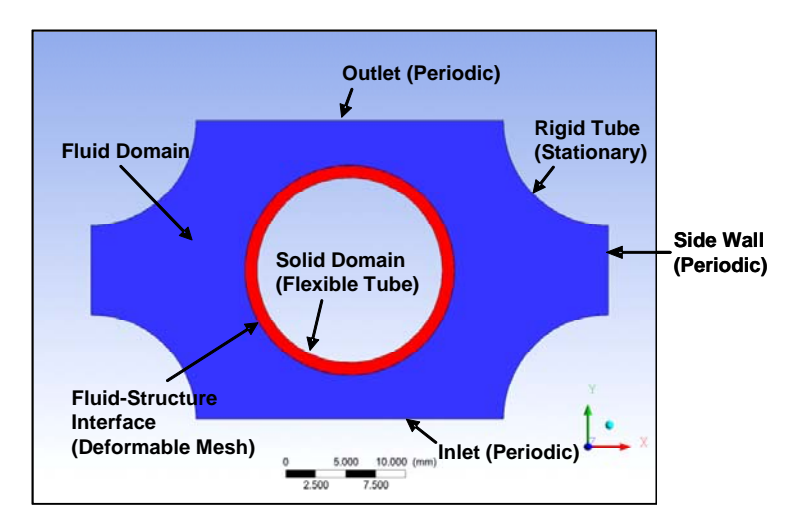


Figure 4 Fluid and solid domains.

2.1.5 Turbulence Model

The k- ω based Shear-Stress-Transport (k- ω SST) model was used to characterize turbulence for demonstrating the onset of fluid-elastic instability, because its simulation times are considerably shorter than other more sophisticated turbulence models such as Scale-Adaptive Simulation (SAS) or Large-Eddy Simulation (LES). A sophisticated turbulence model is not required to demonstrate the onset of fluid-elastic instability, but may be desirable to improve solution accuracy if the unsteady turbulent structures are important to the tube response.

2.2 Results for Onset of Fluid-Elastic Instability

The time-average velocity contours shown in Figure 5 provide an example of the flow field in the computational domain at a superficial velocity of 1.5 m/s, which is obtained from the CFD solution. Although flow enters the symmetrical domain vertically from the bottom boundary, the time-average flow field has triangular wakes behind tubes, which are skewed to the left. The locations of flow separation from the tube surface are rotated approximately 30° counter-clockwise from the symmetrical locations that would otherwise exist behind a single cylinder in crossflow. This phenomenon causes some flow to enter the computational domain through the right-hand boundary (on average) and exit from the left-hand boundary, which is permitted by the translational periodic conditions at these locations. In reality, the wakes exhibit inherently transient behavior and flip-flop from side-to-side as vortices are shed from the tubes, which are observed in the transient flow fields. Skewed or asymmetrical wakes have also been observed in previous experimental [5] and

computational [6] [7] investigations of tube bundles with pitch-diameter ratios less than two. The tube pitch-diameter ratio is 1.43 in the current simulations.

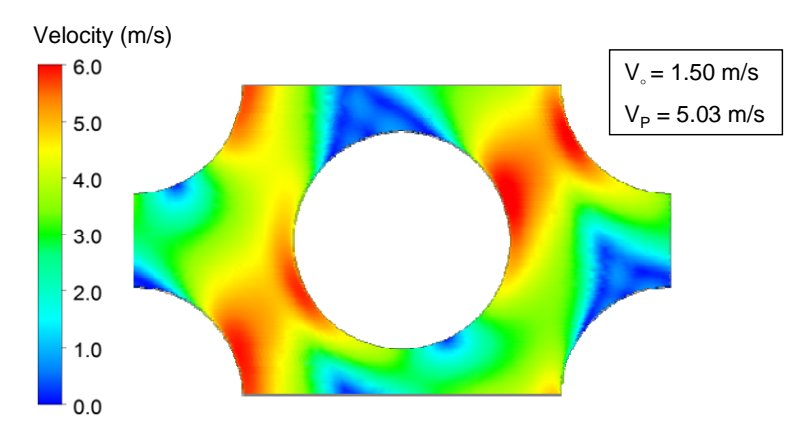


Figure 5 Time-average velocity contours at $V_s = 1.5$ m/s (k- ω model).

The time series of lift forces on the central tube are shown in Figure 6 at superficial velocities (V_s) of 0.75, 1.00, 1.25 and 1.50 m/s. The corresponding drag forces and tube displacements have similar trends. Drag and lift forces are parallel and perpendicular, respectively, to the prevailing flow direction shown in Figure 1, which is the Y-direction of the computational mesh shown in Figure 2. Lift forces are typically in the negative X-direction of the computational mesh. These hydrodynamic forces are obtained by integrating both normal pressures and shear stresses over the entire tube surface, but the normal pressures predominate.

The time series in Figure 6 show that fluctuations in hydrodynamic forces increase in general with increasing superficial velocity and the tube becomes unstable at a superficial velocity of 1.5 m/s where displacements become so large that the flexible tube contacts the neighbouring tubes. Different scales are used on the ordinates of these graphs to accommodate the increasing amplitudes. Origins of the time series are shifted, so the effective transient periods are aligned for more direct comparisons.

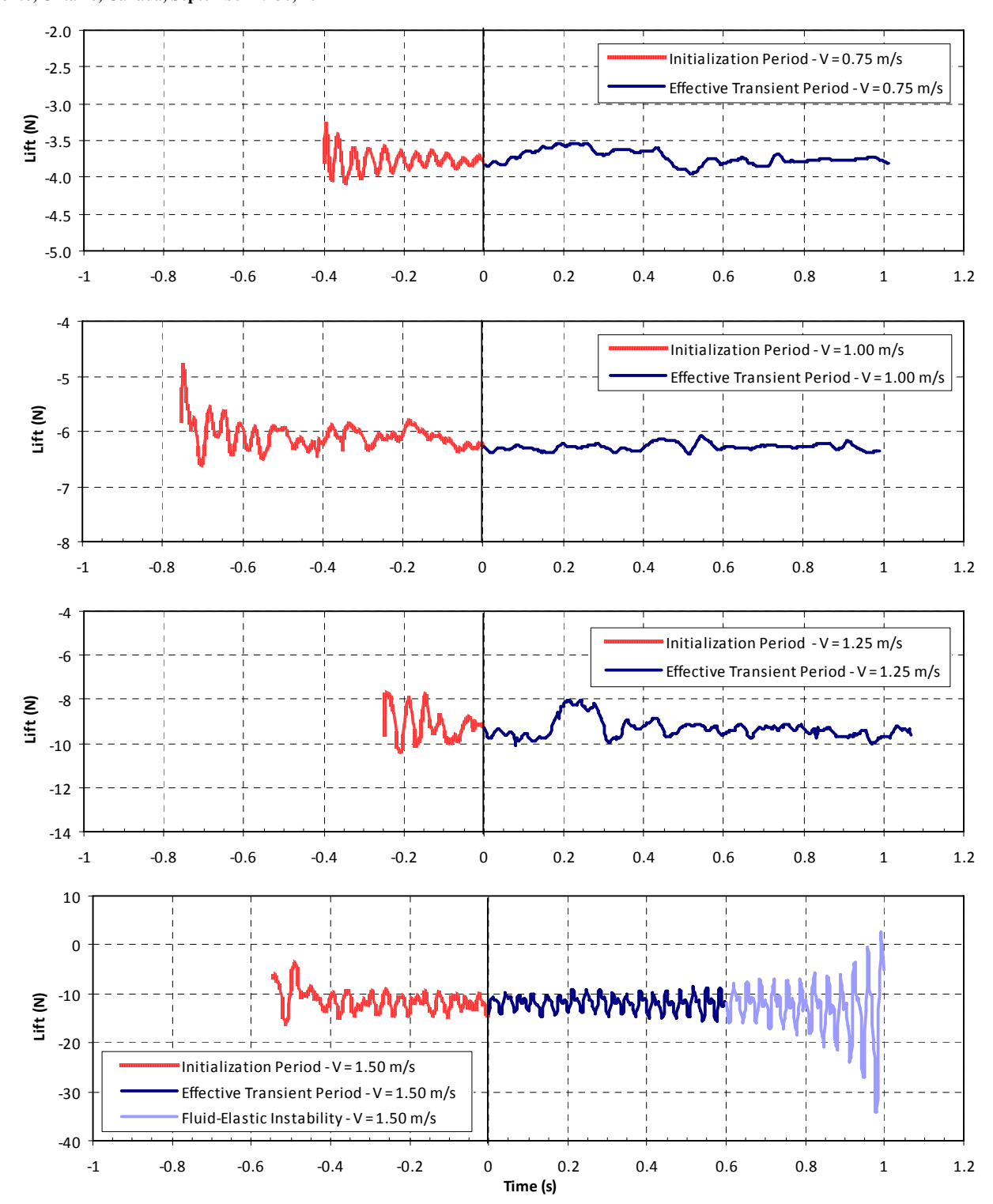


Figure 6 Time series of lift forces at $V_s = 0.75$, 1.00, 1.25 and 1.50 m/s (k- ω model).

The RMS amplitudes of drag and lift forces increase disproportionately by an order-of-magnitude as the superficial velocity is doubled, which indicates the onset of fluid-elastic instability. The RMS lift force is consistently higher than the RMS drag force so fluctuations of tube displacement are higher in the lift (X) direction, which are observed in the orbits of tube displacement in Figure 7. The tube vibrates in a random elliptical path with its major axis predominantly in the lift direction.

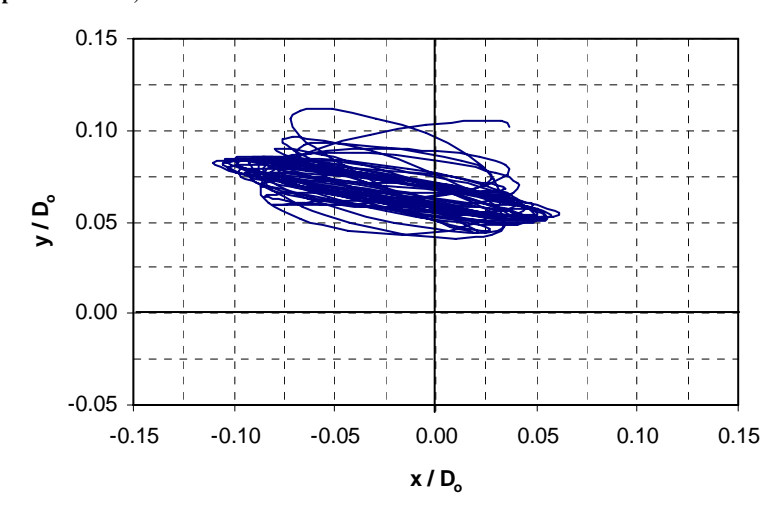


Figure 7 Orbits of tube displacement at $V_s = 1.5$ m/s (k- ω model).

Figure 8 shows how the RMS tube displacements at the monitoring point increase by several orders of magnitude as the superficial velocity is increased from 0.75 to 1.50 m/s, which is further evidence of the onset of fluid-elastic instability. FSI simulations performed at velocities higher than 1.5 m/s did not converge due to the high tube displacements and extreme mesh deformations as the flexible tube contacted the neighbouring rigid tubes.

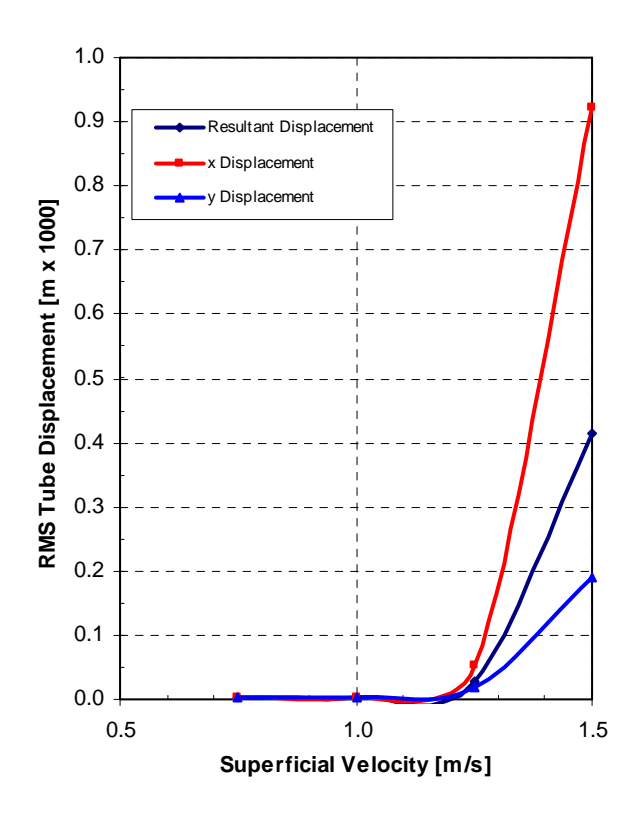


Figure 8 RMS tube displacements (k-ω model).

The dimensionless power spectral density (PSD) distributions of lift forces are shown in Figure 9, which are compared with various envelope guidelines that are considered upper bounds of experimentally measured random forces for a wide variety of tube bundle configurations [5] [8] [9].

The calculated PSD distributions of both drag and lift forces are generally below the envelope guidelines, even at a superficial velocity of 1.5 m/s which becomes unstable at a later time in that simulation.

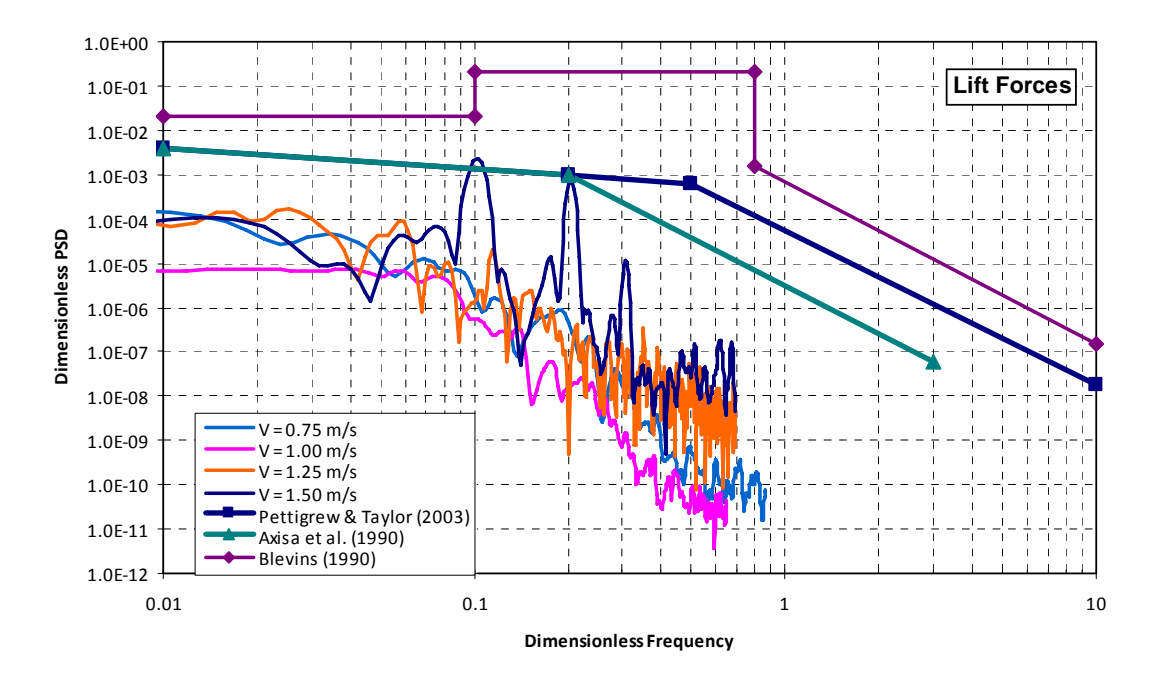


Figure 9 PSD distributions of lift forces at $V_s = 0.75$, 1.00, 1.25 and 1.50 m/s (k- ω model).

Auto power spectral density functions, $S_F(f)$, are calculated from time series of the drag and lift forces for the effective transient periods shown in Figure 6. The PSD functions are non-dimensionalized as follows and plotted with respect to a dimensionless frequency, $\tilde{f} = f D_o/V_P$ for comparison with envelope guidelines:

$$\widetilde{S}_{F}(f) = \frac{S_{F}(f)}{(\rho_{o}V_{P}^{2}D_{o}L/2)^{2}} \frac{V_{P}}{D_{o}}$$
(3)

Figure 9 shows that hydrodynamic forces reside mainly at frequencies less than the fundamental mode of tube vibration, which are significantly attenuated at higher frequencies. There is no evidence of harmonic frequencies in the hydrodynamic forces at low superficial velocities, but dominant peaks are apparent in the PSD distributions of the drag and lift forces at a superficial velocity of 1.5 m/s. The two peaks at dimensionless frequencies of 0.10 and 0.33 are associated with the first and second modes of tube vibration at 29.6 and 95.8 Hz, respectively, which are obtained by modal analysis. The dimensionless frequencies vary with superficial velocity. The peak at approximately 0.21 (59 Hz), between the first two modes, is thought to be spurious, because the k-ω turbulence model causes non-physical, single-mode vortices in unsteady flow fields [10].

Figure 10 shows results of the FSI simulations superimposed on a stability diagram [3], where the dimensionless pitch velocities ($\tilde{V}_P = V_P/f\,D_o$) are plotted at the value of the mass-damping parameter ($\delta_m = 0.34$). Results of the FSI simulations lie above various curve fits of different

Connors' coefficients but close to some of the experimental data points for a rotated triangular array. There is reasonably good agreement in the FSI results, however, considering a coarse computational mesh was used to reduce simulation times. Some of the discrepancy can be explained by the fluid-elastic response of different constrained modes of tube vibration [11], because the tube stability depends on the participation of surrounding tubes. A flexible tube vibrating in a rigid array tends to be more stable than a flexible tube vibrating in a flexible array where other tubes participate in the vibrations. Some of the discrepancy can also be explained by the choice of turbulence model. Larger fluctuations in hydrodynamic forces would be realized using more comprehensive turbulence models such as SAS or LES, which better characterize the unsteady structures of turbulent flows than the k- ω SST model.

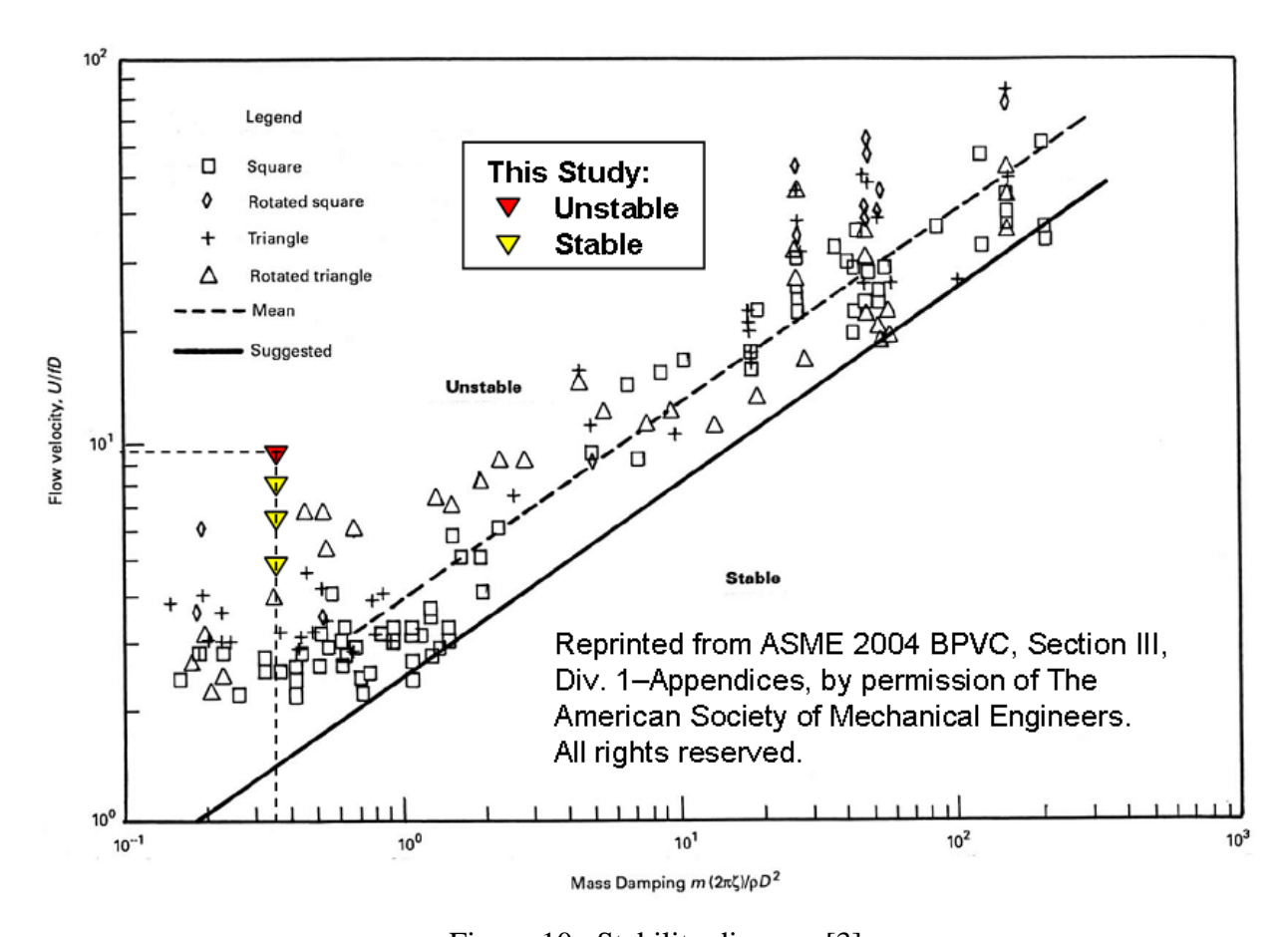


Figure 10 Stability diagram [3].

The damping ratios are calculated using the half-power bandwidth method from the PSD distribution of displacements in the X (lift) direction. These ratios are the viscous damping, which depends entirely on the flow field around the central tube. Material damping of the tube itself is assumed negligible in comparison, and there is no friction or squeeze-film damping at the supports. At a superficial velocity of 0.75 m/s, the average viscous damping is 3.4%, which is close to the upper bound of the mean plus one standard deviation of reported values for heat exchanger tubes (3.06%) [5]. At higher superficial velocities, the average viscous damping is 1.7%, which is midrange of the mean plus or minus one standard deviation of reported values (0.86% to 3.06%). There is therefore very reasonable agreement between the calculated and reported viscous damping, which helps to validate results of the FSI simulations to some extent. Viscous damping depends on the

flow field and therefore the validity of the turbulence model, so results may vary using different turbulence models.

3. Random Turbulence Excitation

3.1 Methodology

The methodology to characterize the response of a flexible tube to random turbulence excitation is substantially the same as that used to characterize the onset of fluid-elastic instability. The computational domain, mesh characteristics, fluid and tube properties, and boundary conditions remain unchanged. Two turbulence models are used: the k-ω model and Scale-Adaptive Simulation (SAS) for better resolution of the unsteady structures of turbulence. One superficial velocity of 0.75 m/s is used, which is below the onset of fluid-elastic instability but should cause discernable tube vibration.

3.2 Results for Random Turbulence Excitation

The time series of lift forces on the central tube and the corresponding tube displacements at the monitoring point are shown in Figure 11 and Figure 12, respectively, for both turbulence models (k- ω and SAS) at a superficial velocity of 0.75 m/s (Re=106,000). Fluctuations in the hydrodynamic forces and tube displacements depend on the turbulence model, which are generally higher with the SAS model. The SAS turbulence model yields much higher fluctuations in dynamic forces than the k- ω model, which are important to characterize the tube response.

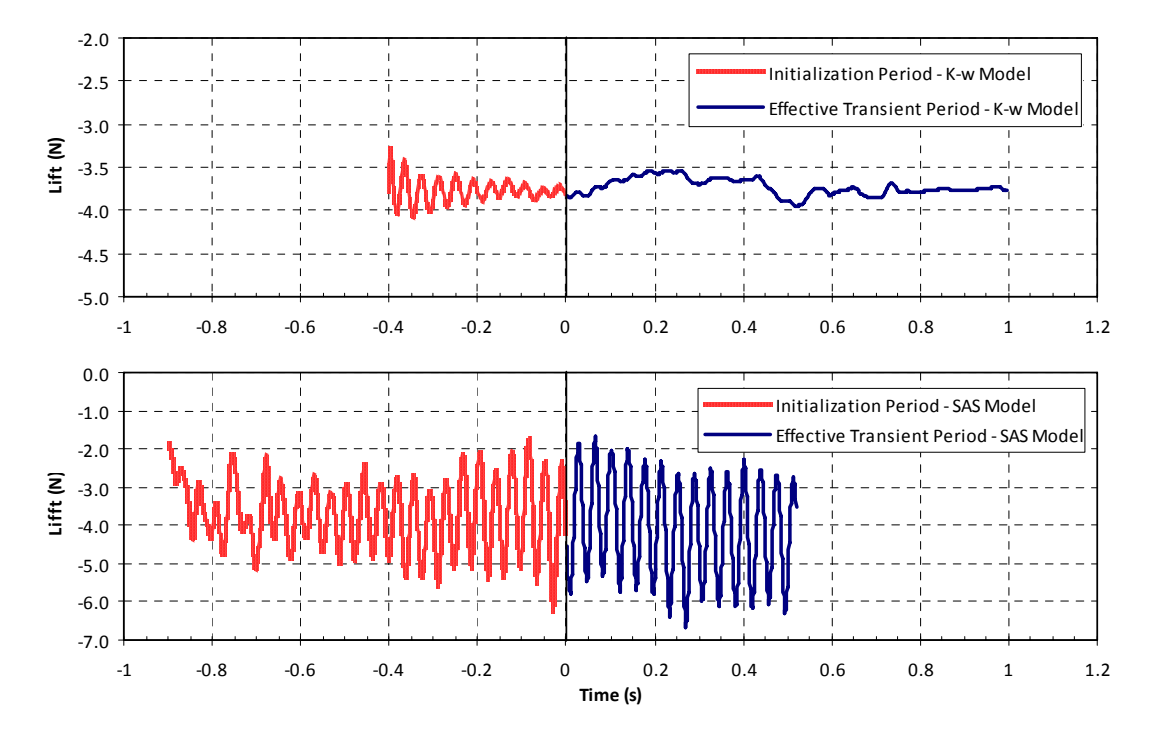


Figure 11 Time series of lift force at $V_s = 0.75$ m/s.

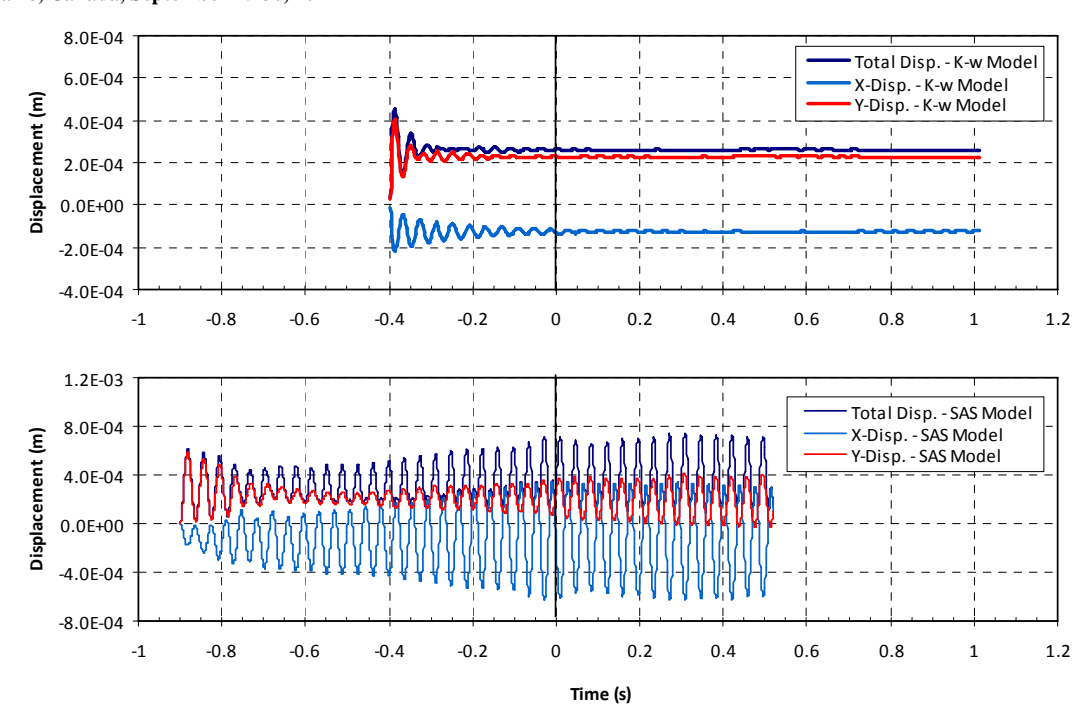


Figure 12 Time series of tube displacement at $V_s = 0.75 \text{ m/s}$

The RMS tube response from the SAS model, however, is two orders-of-magnitude higher than the k- ω model, because the SAS model better represents the dynamic forces. For validation, the RMS tube response is calculated using established empirical equations [12]. The RMS tube response from the empirical model is 0.17 mm, and the SAS results are 0.33 mm and 0.14 mm in the X (lift) and Y (drag) directions, respectively. There is therefore reasonable agreement with empirical correlations for the tube displacement response.

The dimensionless power spectral density (PSD) distributions of lift forces are shown in Figure 13, which are compared with different envelope guidelines [5] [8] [9]. The calculated PSD distributions for both drag and lift forces of the SAS model are significantly higher than those of the k- ω model, because the SAS model better characterizes the unsteady structures of turbulence. PSD distributions of the SAS model also reveal a dominant peak near the first mode of tube vibration, which is not apparent with the k- ω model at a superficial velocity of 0.75 m/s. This dominant peak amplitude may be associated with vortex shedding locking in at the fundamental frequency of the tube.

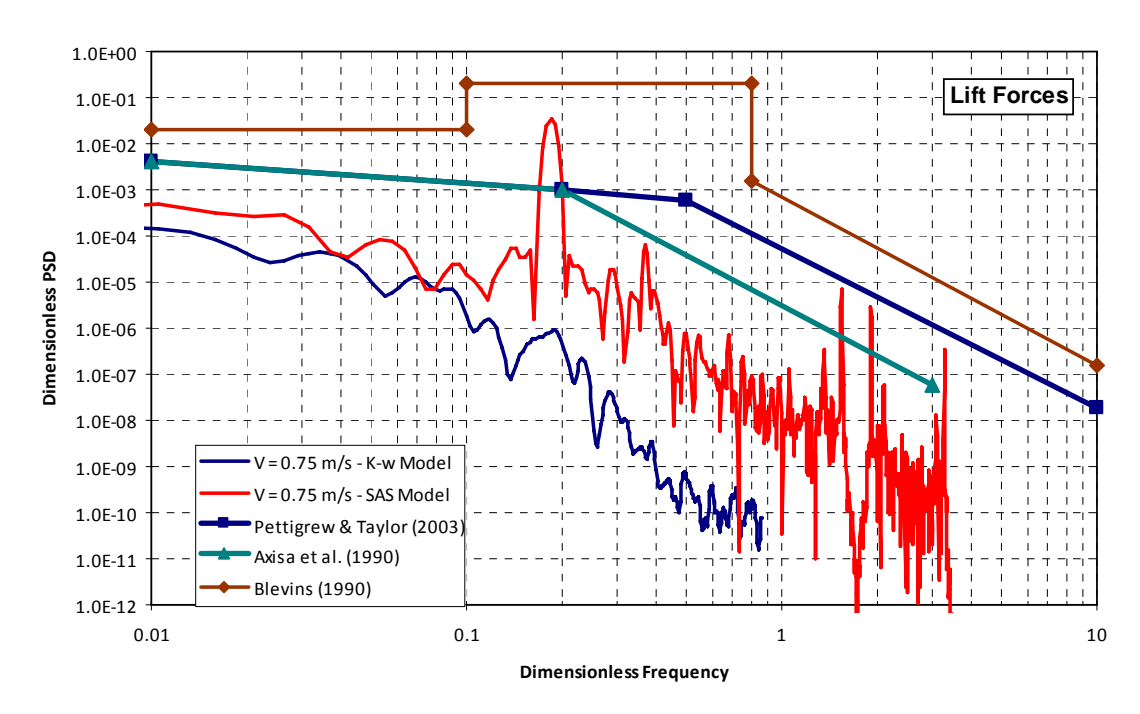


Figure 13 PSD distributions of lift forces at $V_s = 0.75$ m/s.

A viscous damping ratio of 2.2% is calculated using the half-power bandwidth method from the PSD distribution of displacements in the X (lift) direction of the SAS model, which is mid-range of the mean plus or minus one standard deviation of reported values (0.86% to 3.06%) [5]. Material damping of the tube itself (0.11–0.15% [13]) is small in comparison, and there is no friction or squeeze-film damping at the supports. There is therefore very reasonable agreement between the calculated and reported viscous damping, which helps to validate results of the FSI simulations to some extent. Viscous damping depends on the flow field and therefore the validity of the turbulence model. As described in Section 2.2, the average viscous damping is 3.4% at a superficial velocity of 0.75 m/s using the k- ω model, so results vary with different turbulence models.

4. Conclusions

The FSI capabilities of commercial software are demonstrated using two practical examples related to FIV of heat-exchanger tubes, the onset of fluid-elastic instability and the tube response to random turbulence excitation. The intent of these simulations is to validate FSI capabilities for other applications, such as simulating FIV of flexible foreign objects in steam generators. There is reasonable agreement between the FSI simulations and experimental data points on a stability diagram, considering a coarse computational mesh and simple (k-ω) turbulence model were used to reduce simulation times. There is also reasonable agreement in the response to random turbulence excitation using an SAS turbulence model, considering a coarse computational mesh was used to reduce simulation times. Having demonstrated the FSI capabilities of commercial software for modelling typical single-phase FIV mechanisms of heat-exchanger tubes, the software may be used with some confidence to model the dynamic response of flexible foreign objects in tube bundles.

5. References

- [1] K. Schroder and H. Gelbe, "Two- and three-dimensional CFD-simulation of flow-induced vibration excitation in tube bundles", *Chemical Engineering and Processing*, Vol. 38, Issues 4-6, 1999, pp. 621-629.
- [2] K. Kuehlert, S. Webb, M. Joshi and D. Schowalter, "Fluid-structure interaction of a steam generator tube in a cross-flow using large-eddy simulation", <u>Proceedings of the 14th International Conference on Nuclear Engineering (ICONE14)</u>, Miami, FL, 2006, July 17-20.
- [3] American Society of Mechanical Engineers. *Boiler and Pressure Vessel Code*. ASME Publications, New York, NY 2004, Section III, Division 1, Nonmandatory Appendix N, Article N-1000: Dynamic Analysis Methods.
- [4] Hermann Schlichting and Klaus Gersten, *Boundary Layer Theory*, 8th Edition, Springer-Verlag, New York, NY, 2000.
- [5] Robert D. Blevins, *Flow Induced Vibration*, *2nd Edition*, Krieger Publishing Company, Malabar, FL, 2001.
- [6] S. Benhamadouche and D. Laurence, "Large eddy simulation of flow across in-line tube bundles", Proceedings of the 11th International Topical Meeting on Nuclear reactor Thermal-Hydraulics (NURETH-11), Avignon, France, 2005, October 2-6.
- [7] Imran Afgan. *Large eddy simulation of flow over cylindrical bodies using unstructured finite volume meshes*. Ph.D. Thesis Submitted to the University of Manchester, Faculty of Engineering and Physical Sciences, 2007.
- [8] M. J. Pettigrew and C. E. Taylor, "Vibration analysis of shell-and-tube heat exchangers: an overview—Part 1: flow, damping, fluidelastic instability", *Journal of Fluids and Structures*. Vol. 18, No. 1, 2003, pp. 469-483.
- [9] F. Axisa, J. Antunes, and B. Villard, "Random excitation of heat exchanger tubes by cross-flows", *Journal of Fluids and Structures*. Vol. 4, No. 3, pp. 321-341, 1990.
- [10] Y. Egorov and F. Menter, "Development and Application of SST-SAS Turbulence Model in the DESIDER Project", *Notes on Numerical Fluid Mechanics and Multidisciplinary Design; Advances in Hybrid RANS-LES Modelling.* Vol. 97, pp. 261-270, 2008, Proceedings of the 2007 Symposium of Hybrid RANS-LES Methods, Corfu, Greece, 2007, June 17-18.
- [11] S. S. Chen, "Instability mechanisms and stability criteria of a group of circular cylinders subjected to cross-flow. Part 2: Numerical results and discussions", *Journal of Vibration*, *Acoustics, Stress, and Reliability in Design*, Vol. 105, No. 2, 1983, pp. 253-260.
- [12] C. E. Taylor and M. J. Pettigrew, "Random Excitation Forces in Heat Exchanger Tube Bundles", *Journal of Pressure Vessel Technology*. Vol. 122, No. 4, pp. 509–514, 2000.
- [13] M. J. Pettigrew and C. E. Taylor, "Damping of heat exchanger tubes in two-phase flow: Review and design guidelines", *Journal of Pressure Vessel Technology*. Vol. 126, No. 4, 2004, pp. 523-533.